

Effect of liposomal confinement on photothermal and photo-oximetric fluorescence lifetimes of photosensitizers with varying hydrophilicity

Ozzy Mermut
Isabelle Noisieux
Jean-Pierre Bouchard
Jean-François Cormier
Patrice Desroches
Michel Fortin
Pascal Gallant
Sébastien Leclair
Marcia L. Vernon

National Optics Institute
Department of Biophotonics
2740 Einstein St.
Québec, QC, Canada, G1P 4S4
E-mail: ozzy.mermut@ino.ca

Kevin R. Diamond
Michael S. Patterson

McMaster University and Juravinski Cancer Center
Department of Medical Physics and Applied Radiation
Sciences
699 Concession St.
Hamilton, Ontario, Canada L8V 5C2

Abstract. The time-resolved fluorescence of photosensitizers (PSs) of varying hydrophobicities, di- and tetrasulfonated Al phthalocyanines (Al-2 and Al-4), and Photochlor® (HPPH), was investigated in liposomes used as cell-mimetic models. Using frequency- and time-domain apparatus, the fluorescence lifetime, τ_{fluo} , was compared for PSs free in aqueous solution and in a liposome-associated state at varied temperatures (25 to 78°C) and oxygen concentrations (0–190 μM). The analysis of τ_{fluo} revealed different decay behaviors for the free-solution and liposome-confined PSs, most significantly for the lipophilic HPPH. Hydrophilic PS drugs (Al-4, Al-2) were less affected by the liposomal confinement, depending on the relative hydrophilicity of the compound and the consequent localization in liposomes. Changes in the emission decay due to confinement were detected as differences in the lifetime between the bulk solution and the liposome-localized PS in response to heating and deoxygenation. Specifically, hydrophilic Al-4 produced an identical lifetime trend as a function of temperature both *in solu* and in a liposome-confined state. Hydrophobic HPPH exhibited a fundamental transformation in its fluorescence decay kinetics, transitioning from a multiexponential (in free solution) to single-exponential (in liposome) decay. Deoxygenation resulted in a ubiquitous τ_{fluo} increase for all PSs in free solution, while the opposite, a τ_{fluo} decrease, occurred in all liposomal PSs.

© 2008 Society of Photo-Optical Instrumentation Engineers. [DOI: 10.1117/1.2952298]

Keywords: fluorescence lifetime; frequency domain; time domain; photosensitizers; liposomes; photo-thermal; deoxygenation.

Paper 07382SSR received Sep. 14, 2007; revised manuscript received Apr. 7, 2008; accepted for publication Apr. 28, 2008; published online Jul. 10, 2008. This paper is a revision of a paper presented at the SPIE conference on Therapeutic Laser Applications and Laser-Tissue Interactions III, June 2007, Munich, Germany. The paper presented there appears (unrefereed) in SPIE Proceedings Vol. 6632.

1 Introduction

In photodynamic therapy (PDT), tumor-directed cytotoxicity is achieved by either radical intermediates (type I) that are subsequently scavenged by oxygen, or more commonly by the generation of singlet oxygen, $^1\text{O}_2$, (type II). Both pathways are mediated by light activation and energy transfer from a photosensitizer (PS) molecule.^{1–3} Recent work has revealed that localization of PS drugs to different subcellular domains (e.g., membranes, mitochondria, or lysosomes) is correlated to the efficiency of PDT activity.^{4–8} Several *in vitro* investigations of cell cultures also suggest that the charged peripheral substituents (ion type, ionic density) and structure of a PS molecule are correlated to its mode of cell entry, localization, and biodistribution.^{5,9–12} These properties consequently affect the mechanism of cell death achieved with photosensitization (i.e., membrane damage, DNA damage, apoptosis, or necrosis).^{5,7}

The fluorescence lifetime of a PS, τ_{fluo} , provides a way to probe the microenvironment of PS molecules localized in cells.¹³ It describes the average time that photo-excited molecules spend in the singlet state prior to de-excitation. It is of interest to study how the fluorescence decay characteristics are altered with PS hydrophobicity in different microenvironments.¹³ In phthalocyanine-derived PSs, for example, increasing the concentration of PS aggregates (through unfavorable local solvent interactions) leads to shortened singlet- and triplet-state lifetimes, resulting in the reduced production of phototoxic singlet oxygen.^{14,15} Undesired effects on the PS, such as aggregation in low-pH environments (often seen in tumors¹⁶), may be observed through a measurement of the fluorescent lifetime. The advantage of studying τ_{fluo} over steady-state fluorescence is that it serves as a dynamic biochemical probe of the PS in the vicinity of its cellular target, independent of its concentration (in the nonaggregating range).^{16,17} Such information can aid in the design of more efficient PSs optimized for cell-specific targeting, inter-

Address all correspondence to: Ozzy Mermut, Department of Biophotonics, INO, 2740, Einstein St., Québec, QC, Canada, G1P 4S4. Tel: 418-657-7006; Fax: 418-657-7009; E-mail: ozzy.mermut@ino.ca.

nalization, localization, and distribution in the most vulnerable intracellular compartments for PDT.^{2,6,8,18}

While the principles of the photodynamic process are known, mechanistic aspects of photosensitization *in vivo* are not well understood, in part due to the spatial distribution of the PS in cells and the optical heterogeneity of tissues. As such, simplified model systems are desirable to address the primary interactions of PSs within cell-like media. To this aim, one must understand how molecular-scale properties affect photosensitization action in liposomes, which are model constructs designed to structurally, chemically, and optically mimic cells. This is because liposomes can be fabricated on the size scale of 0.05 μm to 1 μm , which imitate subcellular organelles, intracellular chemistry (e.g., lipid and cytosol composition), and cellular interfaces (lamellarity).¹⁹ Much of the work related to liposomes in PDT has focused on their implementation for targeted drug delivery, particularly with hydrophobic photosensitizing agents.²⁰ Recently, the use of liposomes as simplified membrane models has allowed researchers to characterize/identify the influence of physicochemical, photobiological, and biochemical factors on the uptake, aggregation, and distribution properties of PSs in tissues, and the photosensitization mechanism (e.g., parameters such as membrane viscosity, permeability, surface charge density, PS solubility, and binding affinity).^{21,22} By preparing PS-incorporated liposomes with a high level of structural control and reproducibility, we propose that the confinement of PSs in these phantoms can be an effective strategy for probing and predicting the fluorescence decay behavior expected in cells as a function of the PS molecular properties. Previous time-resolved work has demonstrated, for example, singlet- and triplet-lifetime dependence of hydrophobic PS molecules in similar encapsulating systems based on cyclodextran- as calix[n] arenes,¹⁰ as well as PS decay changes in the presence of microbial cells.¹³

Hyperthermia (HT) is a heat treatment during which the temperature of the tissue is elevated artificially with the aim of achieving a therapeutic effect. The heating of tissue may alter the structure (e.g., through denaturation) and physiology of the tissue of interest; the changes in blood flow that result from heating are the most relevant effect when considering the outcome of PDT.^{23,24} It has been demonstrated that the combination of HT and PDT increases the overall cytotoxic efficiency of the method.^{25–27} The proliferation of tumor cells results in a reduction of vascular density, disorganization of the vascular network and structure, and compositional changes in the extracellular matrix. These modifications to the tumor microenvironment limit the delivery of drugs to cells that are situated distally from functioning blood vessels, leading to the inefficient uptake of macromolecules and reduced mobility in tumor cells. During HT treatment, vasodilation occurs. When this is combined with a liposome drug-delivery approach, it facilitates extravasation of the PS-bearing liposomes into the tissue of interest.²⁴ In some applications, the temperature-sensitive release of a drug from liposomes allows tumor cells to be exposed to much higher concentrations.²⁸ Thus, the delivery of a PS in a liposome format can significantly increase the therapeutic ratio in temperature-mediated photodynamic action.²⁸

Relevant to treatment and diagnostics, local oxygen concentration and temperature are two important parameters for

in vivo photosensitization. During the photodynamic treatment of tissues, oxygen is depleted due to (1) the consumption of molecular oxygen through production of $^1\text{O}_2$ and its irreversible reactions with biomolecules; and (2) the decreased supply of blood and oxygen in the tumor caused by damage to the vasculature in and around the tumor.^{23,29,30} The efficiency of photosensitization is directly related to the yield of $^1\text{O}_2$ in the tumor environment and can depend on the concentration of external oxygen available. Hypoxic cells having less than 5% oxygen exhibit resistance to PDT.⁷ Oxygen concentration can decrease during PDT light delivery if the tissue oxygen supply is restricted, potentially leading to inadequate treatment. Cells contain many quenchers, and singlet oxygen can diffuse between 20 nm and 100 nm.^{1,31} For an energy transfer reaction to occur, $^3\text{O}_2$ and the sensitizer must be in close proximity.⁷ The physicochemical properties of an intracellular PS are thus closely linked to the efficiency of oxygen-mediated energy transfer in the PS local environment. Tracking τ_{fluor} of PSs at various oxygen concentrations provides mechanistic insight into photosensitization as a function of spatial confinement in simplified but realistic cell-like phantoms.

In the companion to this work, it was demonstrated that for a PS molecule of a given concentration, its hydrophilic/hydrophobic properties dictated its aggregation behavior.³² Absorbance and fluorescence spectra of solution-phase PSs, compared to those confined in liposome cell models, showed the photochemical consequences of chemically driven localization into different liposome domains for Al-2 (aluminum phthalocyanine disulfonate chloride), Al-4 (aluminum phthalocyanine chloride tetrasulfonic acid), and porphyrin-based HPPH (2-(1-hexyloxyethyl)-2-devinyl pyropheophorbide): the PS amphiphilicity resulted in the preferential localization of drug molecules in specific microenvironments of liposomes, where they adopted different aggregation behaviors.

The consequences of PS localization on the fluorescence decay in response to temperature and oxygenation may be important to the understanding and interpretation of changes in the action of the PS. In the present study, the kinetics of the fluorescence decay were investigated using a hybrid frequency-domain/time-domain apparatus with excitation sources of 661 and 400 nm, respectively. Fluorescence lifetime was resolved in both domains by expressing the decay as a summation of exponential terms. We acquired the relative phase response (frequency-domain) and the fluorescence decay curves (time-domain) as a function of increasing temperatures and variable oxygen concentration. Our aim was to resolve the differences in the τ_{fluor} response function in solution-phase PSs versus those localized within cell-mimetic liposomes.

2 Materials and Methods

2.1 Materials

Three PSs were investigated: aluminum (III) phthalocyanine chloride tetrasulfonic acid (Al-4, Frontier Scientific, Incorporated, UT, USA), aluminum (III) phthalocyanine disulfonate chloride adjacent isomer (Al-2, Frontier Scientific), and 2-(1-hexyloxyethyl)-2-devinyl pyropheophorbide, HPPH, kindly provided by the Roswell Park Cancer Institute. PS solutions

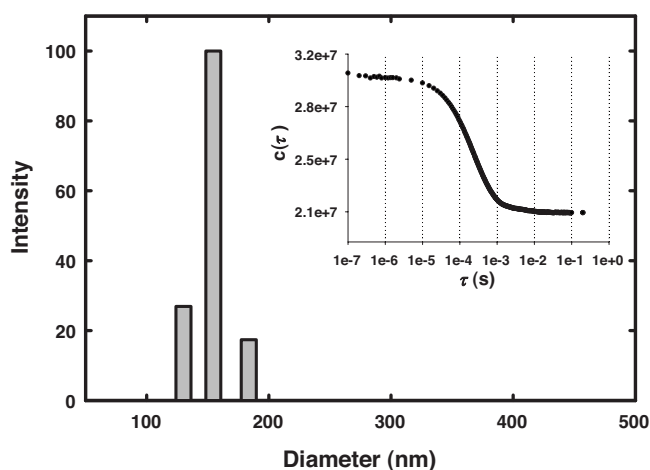


Fig. 1 Typical intensity-based distribution of the hydrodynamic diameter of "100-nm" L-PS and L-Blank as measured from the DLS autocorrelation function (inset).

were prepared in phosphate-buffered saline (PBS, pH 7.4) for the AI-2 and AI-4, and 20:80 fetal bovine serum (FBS)/PBS (Sigma) for the HPPH. All samples were prepared using 0.45- μm filtered, deionized water (UV-treated 18.2 M Ω ·cm resistivity). Liposomes were prepared with 1,2-dioleoyl-*sn*-glycero-3-phosphocholine (DOPC) and cholesterol (CHOL, Northern Lipids Incorporated, B.C., Canada). Sephadex G-25 columns were used for size exclusion separation (NAP 5, GE Healthcare).

2.2 Liposome Preparation Incorporating PS

Details of the liposomes' preparation were reported in the companion to this work.³² Briefly, PS incorporation into liposomes was achieved by hydration of a thin lipid cake (composed of DOPC and 35% CHOL) with one 50- μM AI-4, 25- μM AI-2, or 100- μM HPPH. The suspension was then subjected to freeze-thaw cycles, followed by extrusion through a 100-nm polycarbonate membrane. Separation of free PS (bulk solution) from liposome-confined PS (L-PS) was achieved by size exclusion. Vesicle size for all L-PSs and blank liposomes (L-Blank) was determined from dynamic light scattering measurements (DLS) acquired at varying angles between 90 and 150 deg (a BI9000 apparatus from Brookhaven Instruments at 532 nm using a BI200SM goniometer and a B2FBK/RFI PMT).³³ DLS measures the time variation of the scattered light intensity, which is analyzed by the intensity autocorrelation function acquired from a digital correlator, described previously.³⁴ The intensity autocorrelation function is the ensemble average of the product of the signal with a delayed version of itself as a function of the delay time (inset Fig. 1). Each population of particle size produces its own unique contribution to the autocorrelation function, allowing for the determination of the distribution or uniqueness of the size distribution. A diffusion coefficient is derived using the Stokes-Einstein relation, which relates the diffusion coefficient to the hydrodynamic radius of the particle according to $D = K_b T / 6 \pi \eta R$, where K_b , T , and η are Boltzmann's constant, temperature, and viscosity, respectively. The algorithms used to analyze the autocorrelation

function and extract the size distribution were non-negative constrained least square (NNLS) and CONTIN (a method suitable for analyzing polydisperse populations where the autocorrelation function is examined through an inverse Laplace transform).³⁴ The liposome (scattering) concentration was matched for all L-PS solutions to $2.7 \times 10^7 \text{ mL}^{-1}$ as determined by flow cytometry. The characterization of fluorescence and absorption spectra of the solutions was discussed previously in the companion to this work.³²

2.3 Temperature and Deoxygenation Experiments

Temperature control of the fluorescence cell was achieved using a thermal water jacket linked to a thermo-regulated circulating water bath. Lifetime measurements were acquired in 2 to 5 $^\circ\text{C}$ increments ramping from 26 to 78 $^\circ\text{C}$. An observed deviation of 1 $^\circ\text{C min}^{-1}$ yielded a maximum uncertainty of $\pm 1^\circ\text{C}$ over the course of each measurement. Differential scanning calorimetry (DSC, Seiko, DSC 6200) was performed for L-HPPH and L-Blank (75 mg at a liposome concentration of $8 \times 10^7 \text{ mL}^{-1}$) in a nitrogen-purged environment covering the temperature range of the lifetime measurements (ramp rate of 5 $^\circ\text{C min}^{-1}$, referenced to the solvent of identical mass).³⁵ For deoxygenation studies, ambient samples (having equilibrium concentration of dissolved oxygen at standard temperature pressure (STP) were purged with inert Ar gas at a flow rate of 150 mLmin $^{-1}$ for 3 min to avoid mechanical stress to the liposomes. The dissolved oxygen concentration was quantified using an oxygen probe (model DO-166MT-1, Lazar Research Laboratories Inc.)

2.4 Frequency-Domain Lifetime Instrument and Measurements

The frequency-domain (FD) system was based on phase and amplitude measurements acquired from a network analyzer (Agilent 8753D, 30 kHz to 3 GHz).³⁶ The radiofrequency (RF) output of the network analyzer was used as the external modulation input of a 661-nm diode laser (PicoQuant, 100 kHz to 2 GHz, LDH-M-C-650B) and an MDL300 driver (PicoQuant). A variable attenuator and a $660 \pm 5\text{-nm}$ laser-line filter (Omega Optical) were used at the output of the laser. A small fraction of the laser light was directed to a high-speed positive-intrinsic-negative (PIN) photodiode (1601 New Focus, 30 kHz to 1 GHz) prior to injection into a 600- μm core multimode optical fiber (numerical aperture = 0.37, Thorlabs, MD29L01). The electrical signal from the PIN diode was connected to the reference input of the network analyzer to provide a reference signal. The distal end of the excitation optical fiber was brought in contact with the wall of a 1-cm quartz fluorescence cuvette (Starna Cells) in a fixed geometry. An identical optical fiber, set at 90 deg on the adjacent side of the cuvette, was used for fluorescent light collection. The output of the collection fiber was collimated (Edmund Optics, aspheric lens, 47726), filtered with a 40-nm-wide bandpass filter centered at 690 nm (Semrock OD 5) and focused onto an avalanche photodiode (APD) detector (Hamamatsu C5658, 50 kHz to 1 GHz). The electrical signal from the APD was sent to the input of the network analyzer, and the complex ratio of the APD:PIN phase signal was acquired. Each measurement was an average of 3 scans acquired over 45 s with the network analyzer set to a narrow interme-

diate focus (IF) bandwidth (30 Hz) for optimal noise reduction. Expressing the fluorescence decay as a sum of exponential decays, the frequency-dependent response can be represented in complex notation as

$$H(\omega) = \sum_i \frac{A_i}{1 + j\omega\tau_i}, \quad (1)$$

where A_i is the DC amplitude of the i^{th} component having associated lifetime τ_i . The phase response is given by

$$\varphi(\omega) = \tan^{-1} \left\{ \frac{\text{Im}[H(\omega)]}{\text{Re}[H(\omega)]} \right\}, \quad (2)$$

where the real and imaginary part of $H(j\omega)$ can be computed from Eq. (1), thus giving

$$\text{Re}[H(\omega)] = \sum_i A_i \frac{1}{1 + \omega^2 \tau_i^2}$$

and

$$\text{Im}[H(\omega)] = \sum_i A_i \frac{-\omega\tau_i}{1 + \omega^2 \tau_i^2}. \quad (3)$$

Unless otherwise stated, phase measurements were fitted to a single exponential lifetime model using least-square fitting over the frequency range of 0.1 to 100 MHz. The goodness of the single exponential fit was determined by examining the reduced chi squared, χ_R^2 , computed from the residuals.³⁷

2.5 Time-Domain Lifetime Instrument and Measurements

For samples exhibiting multiexponential decay or low quantum yield, additional measurements of the lifetime were acquired in the time-domain (TD) using time-correlated single-photon counting (TCSPC). The excitation source was a thermoelectrically cooled 400-nm picosecond laser diode (PicoQuant GmbH, Germany) with a pulse duration of ~ 150 ps and a repetition rate of 40 MHz. The laser pulse was delivered to the measurement cell, shared with the FD system, using a multimode 600- μm optical fiber. A variable neutral density attenuator placed in front of the fiber coupler controlled the laser power delivered to the sample. A 90-degree configuration was used to capture fluorescence with a second fiber. The fluorescence collection fiber was coupled to a photon-counting photomultiplier tube (PMT, PMH-100, Becker-Hickl, Germany) with an aspheric lens (Edmund Optics 47726) for collimation. A 670- to 710-nm bandpass interference filter, positioned in front of the photocathode, rejected the excitation light. The PMT output was connected to an SPC-730 TCSPC peripheral component interface (PCI) board (Becker-Hickl, Germany) synchronized with the laser driver trigger signal as the reference. The time window was set to 25 ns for all measurements based on the laser pulse repetition frequency. Fluorescence and background signal acquisition times were set to 180 s as a compromise between maximizing the photon counts (to increase SNR) and minimizing the sedimentation of liposomes (to reduce optical heterogeneity).

A system response function (SRF) trace was acquired with an empty sample cell before each measurement set to account for its effect on the raw measurements. Additionally, in scattering samples, the scattering contribution (convolved in the SRF) was determined through an independent measurement of blank liposomes of equal concentration. The fluorescence lifetime was obtained from the measurements by fitting a single or double exponential model of fluorescence decay to the data, represented by the impulse response function, $I(t)$:

$$I(t) = \sum_i A_i e^{-t/\tau_i}, \quad (4)$$

where A is the pre-exponential factor, and τ_i is the lifetime of the i^{th} component at time t .³⁷ Where necessary, the background was subtracted from the raw data (e.g., FBS/PBS solvent). The measured SRF was then convolved with the exponential decay model and fitted to the processed data using a weighted least-squares approach based on the Levenberg-Marquardt algorithm.³⁸ The choice of single or dual exponential model was evaluated by comparing the χ_R^2 results from both models. A two-fold decrease in χ_R^2 upon incrementing the model from single to dual exponential served as the criterion to add a second decay component. A ratio of χ_R^2 values ≥ 2 is adequate to reject the simpler single exponential model with 99% confidence.³⁷

3 Results

3.1 Size and Shape of PS-Confined Liposomes

Various analysis methods of the DLS autocorrelation function $C(\tau)$ (inset Fig. 1) were used to determine and compare the vesicle sizes and distributions (e.g., CONTIN, NNLS, and Gaussian).³⁹ The intensity-weighted results predominantly showed a single vesicle population of a narrow size distribution for the targeted “100-nm” L-HPPH, L-AI-4, L-AI-2, and L-Blank of actual size $\sim 134 \pm 45$ nm. Figure 1 shows a typical histogram derived from $C(\tau)$ (inset) for all “100-nm” extruded L-PSs and L-Blanks, independent of the PS type. Size results from 100-nm particles were model independent (typical residuals RMS error $\leq 1.5 \times 10^{-3}$) with some minor aggregate contributions at measurement concentrations, 0.1% by mass. DLS measurements as a function of angle showed identical results within error, suggesting a spherical shape for all vesicles.

3.2 Lifetime of Solution Phase Versus Confined PS and Temperature Effects

The phase-derived τ_{fluo} response to increasing temperature was measured and compared for solution-phase PS versus L-PS. The phase curve was acquired for each sample solution starting at ambient conditions ($T=23^\circ\text{C}$, and equilibrium oxygen in solution) and ramping to 78°C . The fitted values of τ_{fluo} of all three PSs free in bulk solution and confined in liposomes are summarized in Table 1 along with the corresponding errors. Separate sample cells were employed in the measurements of τ_{fluo} for temperature and oxygen experiments in the FD. Relative changes in the fluorescent lifetime were examined using a constant geometric setup in each analytical series to examine either temperature or oxygen effects.

Table 1 Summary of the FD fluorescence lifetime results (and relative fluorescence) of free-solution PS (bulk) versus L-PS in ambient, deoxygenated, and heated environments.

PS	Bulk τ (ns)			Confined τ (ns)			
	τ	τ_{-O_2}	$\Delta\tau_{\text{heat}}$ (RT to max T) ^a	τ	τ_{-O_2}	Norm DC M (Amb: -O ₂)	$\Delta\tau_{\text{heat}}$ (RT to max T) ^a
Al-2	5.99±0.01	6.03±0.01	-0.04±0.01	5.47±0.02	4.94±0.02	1:0.79	-0.18±0.01
Al-4	7.64±0.02	7.71±0.02	-0.34±0.02	6.23±0.01	5.99±0.01	1:0.66	-0.35±0.01
HPPH ^b	5.65; 1.1	5.78; 1.23	0.15	7.67±0.01	7.62±0.01	1:0.92	-1.02±0.01
Blank fluo. ^c	—	—	—	8.21±0.05	8.20±0.06	—	—
Blank scatt. ^d	—	—	—	0.06±0.001	0.06±0.001	—	—

^aMaximum χ^2 and error bars reported for the entire temperature series.

^bResults of multiexponential fit for longer-lived species.

^cAutofluorescence signal is less than 0.11% of the total signal (fit to 15 MHz).

^dScattering signal (fitted to 600 MHz).

For each data point, error bars were estimated using a well-established Monte Carlo method.⁴⁰ This technique consists of building a hypothetical data set of $N=100$ lifetime measurements by adding Gaussian noise to the theoretical phase model (calculated using the experimentally determined lifetime). The noise level used was estimated from the residuals of the fit to the experimental data. The theoretical phase model was then fitted to each hypothetical measurement using the same Levenberg-Marquardt routine to obtain a distribution of lifetimes. Twice the standard deviation of the N -fitted τ values were reported as errors to reach a 95% confidence level. Worst-case error bars, as reported herein, were $\leq \pm 0.02$ ns.

The change in goodness of fit (biexponential for HPPH) can be assessed by noting that the χ_R^2 value decreased by a factor ≥ 2 upon confinement of the free PS into L-Al-4 and L-HPPH but increased two-fold as a consequence of L-Al-2 confinement. The measured fluorescence lifetimes of Al-2 and Al-4, presented in Figures 2(a) and 2(b), decreased with increasing temperature due to the increased nonradiative collisional relaxation processes. An exception to this was observed in the solution phase of HPPH [Fig. 2(d)] the exhibited two lifetime components, which both increased with increasing temperature.

Since liposomes scatter light, the “apparent” lifetime introduced by photon migration arising solely from liposome scattering was also measured in the FD using L-Blank. The scattering configuration was identical to the fluorescence measurement geometry but without a fluorescence filter; the modulation frequency range was extended to 600 MHz. The “scattering lifetime” of L-Blank was collected at the identical particle concentration, particle size, and temperature range as that of L-PS and found to be ≤ 0.06 ns (Table 1). The scattering lifetime over the temperature range was found to vary between 0.03 and 0.06 ns.

For solution-phase Al-2 [filled circles in Fig. 2(a)], a small net decrease in τ_{fluo} of 0.04 ns was observed upon heating (Table 1). This temperature dependence was observed up to 47°C, above which τ_{fluo} stabilized. The fluorescent lifetime of the liposome-confined state also decreased [empty circles,

Fig. 2(a) and Table 1], but the magnitude was larger (0.18 ns). Furthermore, unlike the solution-phase response, the decrease was continuous over the entire temperature range. In the case of the tetrasulfonated analog, heating of Al-4 (free in solution) resulted in lifetime shortening identical to that observed for L-Al-4 (by 0.34 and 0.35 ns, respectively). While the lifetime values differed by approximately 1.3 ns, the temperature response curves of both Al-4 and L-Al-4 were both linear ($R^2 > 0.99$) and had the same slope (-0.01 ns°C⁻¹), as evident in Fig. 2(b).

A comparison of the τ_{fluo} response of HPPH [filled symbols, Fig. 2(d)] and L-HPPH [empty symbols, Fig. 2(c)] revealed a remarkably different response to heating. First, it is noteworthy that the phase curve obtained at all temperatures from HPPH in bulk solution did not fit a monoexponential decay model. Employing a biexponential model resulted in a more suitable fit, as evaluated by a reduction in the χ_R^2 value by a factor of 8. However, upon liposome encapsulation, we observed that the decay kinetics of L-HPPH collapsed to a single exponential with good fit ($\chi_R^2 \sim 1.69$) across all temperatures. The raw phase data illustrate a significant difference between the lifetime decay responses for HPPH and L-HPPH (Fig. 3), as shown at the extremes of the temperature range. Examination of the temperature-dependent phase shift suggested that the fluorescence decay of HPPH *in solu* may not be purely biexponential over the entire temperature range since the shape of the phase curve changed (Fig. 3, solid lines). A complementary TD measurement acquired for solution-phase HPPH (inset Fig. 3) demonstrated the multiexponential nature of the decay. Solvent autofluorescence (20:80 FBS/PBS) from 400-nm excitation was measured as $\leq 1\%$. Conversely, TD acquisitions of L-HPPH showed reproducible adherence to a monoexponential decay from 23 to 78°C, despite additional autofluorescence from the liposome membrane when excited at 400 nm (inset Fig. 3). Independent examination of the autofluorescence from L-Blank samples ($\tau_{\text{autofluo}}=8.2$ ns; Table 1) revealed a negligible background contribution to the decay of L-HPPH due to 400-nm excitation in TD.

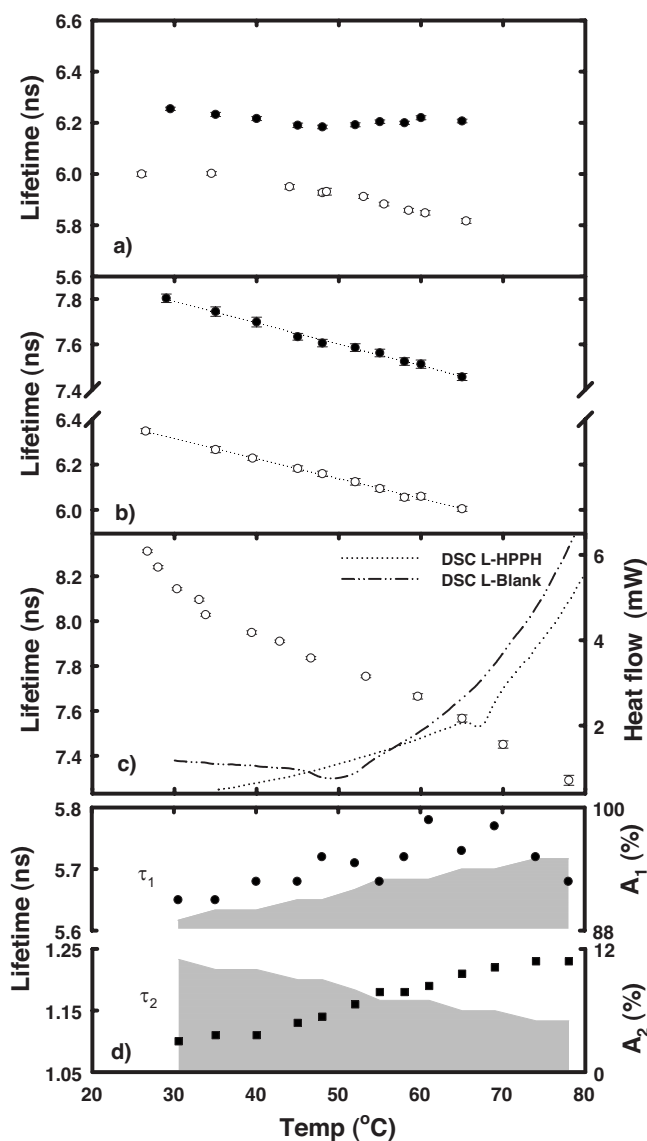


Fig. 2 FD τ_{fluo} fits (with error bars) at temperatures ranging from 25 to 78°C for the bulk PSs (filled symbols) versus liposomal PSs (empty symbols) for: (a) Al-2, and (b) Al-4. (c) L-HPPH measured lifetimes are shown with the DSC traces (right axis) of L-Blank and L-HPPH liposomes embedded. (d) τ_{fluo} of the free-solution HPPH (filled symbols) and the pre-exponential amplitude in shaded areas (A_1, A_2), representing the fractional contribution of photosensitizer associated with τ_1 and τ_2 , respectively.

Unlike the phthalocyanines, the direction of the temperature-induced phase shifts for solution-HPPH and L-HPPH were opposite one another, as illustrated in Fig. 3 (raw data) and shown in the fitted results [Figs. 2(c) and 2(d)]. A significant decrease of 1.02 ns in the fluorescence lifetime was observed upon heating L-HPPH [Fig. 2(c); Table 1]. However, Fig. 2(d) shows that a small increase in lifetimes (average $\Delta\tau_{\text{fluo}} \sim 0.15$ ns) resulted from heating solution-phase HPPH as τ_1 increased from 5.65 to 5.78 ns and τ_2 increased from 1.1 to 1.23 ns. The lifetime increases were accompanied by a change in the respective pre-exponential amplitudes: A_1 increased from 89 to 95% while A_2 decreased

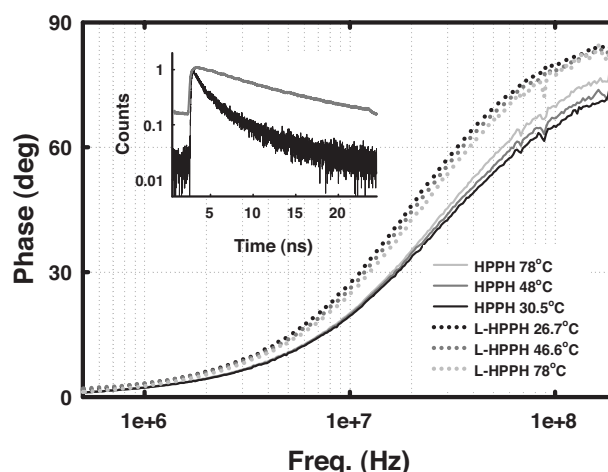


Fig. 3 Typical FD fluorescence phase shift measured over a range of temperatures comparing bulk HPPH (solid lines) and L-HPPH (dotted lines). Inset shows the TD multi- and mono-exponential decay curves at 400-nm excitation of bulk HPPH (black) and offset L-HPPH (gray), respectively, in agreement with FD results.

from 11 to 5%, representing a change in the relative contribution of the long- and short-lived components.

The lifetime data, in corroboration with the spectroscopic results explained in the companion work,³² provide evidence that HPPH localization to the liposome membrane changes its photochemical and photodynamic properties. To examine the impact of confining a PS on the thermal phase behavior and fluidity of the membrane, DSC was performed on L-HPPH and L-Blank. We observed a significant shift in the phase transition peak of liposome vesicles from 50°C (L-Blank) to 67°C (L-HPPH) due to the incorporation of HPPH into the liposomes.

3.3 Lifetime Response of Solution Phase versus Confined PS to Deoxygenation

The efficiency of deoxygenation in PS and L-PS solutions was verified by measuring a three-orders-of-magnitude reduction in the concentration of dissolved oxygen upon changing from ambient ($190 \mu\text{M}$, $\pm 0.1\%$) to Ar-purged ($0.19 \mu\text{M} \pm 0.1\%$) conditions. The fitted values of τ_{fluo} of all three PSs free in bulk solution and confined in liposomes, along with values for blank liposomes (controls), are summarized in Table 1 along with the corresponding errors. To identify τ_{fluo} changes attributed to deoxygenation of confined PSs, it is necessary to consider the lifetime response of the background, L-Blank, to oxygen concentration at comparable vesicle size (~ 134 nm) and concentration ($2.7 \times 10^7 \text{ mL}^{-1}$) as the L-PS. The τ_{autofluo} of L-Blank was measured in the FD and found to contribute $< 0.1\%$ of the magnitude of the L-PS fluorescence signal with 661-nm excitation. The Fig. 4 inset shows overlapping phase traces for ambient and deoxygenated L-Blank with nearly identical results, $\tau_{\text{autofluo}} = 8.21 \pm 0.05$ ns and 8.20 ± 0.06 ns, respectively. As before, the scattering contribution to the lifetime was ascertained from phase fits to 600 MHz, yielding 0.060 ± 0.001 ns in both ambient and deoxygenated environments (Table 1). The low values for χ_R^2 in the fits for scattering and autofluores-

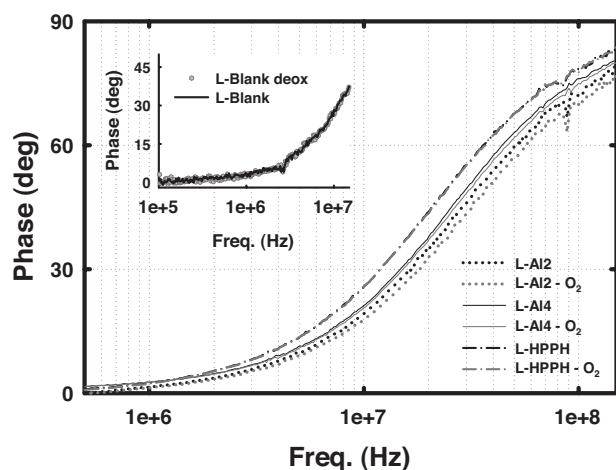


Fig. 4 Typical FD fluorescence phase shift at ambient (black curves) and deoxygenated (gray curves) conditions for L-PSs: L-Al-2 (dotted), L-Al-4 (solid), and L-HPPH (dash-dot). Inset shows blank liposomes under ambient and deoxygenated conditions, with overlapping traces.

cence lifetime of L-Blank (between 0.1 and 0.22) suggested good adherence of both measurements to a single exponential description (Table 1).

Similar to the temperature series, $\Delta\tau_{\text{fluo}}$ due to deoxygenation of the solution-phase PS was examined and compared to the confined L-PS (Table 1). A small but reproducible increase in τ_{fluo} (0.04 to 0.16 ± 0.02 ns) was observed in all cases of deoxygenating free-solution PS. As shown in Fig. 4, the lifetime shifts induced by deoxygenation of the confined L-PS were remarkably different: in the case of L-Al-2 and L-Al-4, we obtained a significantly lower lifetime (decreases of 0.53 and 0.24 ns, respectively) with Ar-purged solutions; the effect in L-HPPH was less pronounced, where a reduction of 0.05 ± 0.01 ns was observed. Deoxygenation of all L-PS solutions also resulted in a reduction in the magnitude of the fluorescence signal, M (TD and FD). This effect was most pronounced in hydrophilic L-Al-4 ($M_{\text{Amb}}:M_{-02}=1:0.79$) and amphiphilic L-Al-2 ($M_{\text{Amb}}:M_{-02}=1:0.66$), where M_{Amb} and M_{-02} represent the fluorescence magnitude under ambient and deoxygenated conditions. Unlike the other L-PSs examined, the χ_R^2 value increased by a factor of 1.5 upon deoxygenation of L-Al-2, suggesting some deviation from a monoexponential model due to deoxygenation. Hence, we evaluated the validity of the deoxygenation results by examining the raw phase data in ambient versus deoxygenated media. Figure 4 shows that the phase curve of L-Al-2 is clearly right-shifted in phase upon deoxygenation, indicative of lifetime shortening, which agrees with the fitted results. Similarly, deoxygenation produced a visually discernable reduction in τ_{fluo} in the case of L-Al-4. The overlap of the phase traces for ambient and deoxygenated L-HPPH suggests that the lifetimes are similar and cannot be discriminated without fitting the data.

4 Discussion

4.1 Localization of Photosensitizers in Liposomes

The efficiency of a PS depends on its subcellular localization. As explained the companion work,³² fluorescence microscopy can be used to identify spatial confinement of a PS in lipo-

somes. The spectral consequences of confining three PSs of varying hydrophobicity, Al-2, Al-4, and HPPH, in liposome phantoms were examined the companion work.³² It was evident that the hydrophilic nature of the PS molecule controlled the relative partitioning of PS in the cell-like constituents of liposomes. This preference for lipid versus aqueous domains also has consequences on the entry mechanism and diffusion of PSs within cells. For example, a lipophilic PS (e.g., HPPH) can diffuse to the membrane of intracellular organelles,⁴¹ while hydrophilic PSs usually enter the cell via an active endocytotic mechanism with preference for polar locations in the cell.² Given our recent spectroscopic findings of the effects of PS confinement in liposomes, our objective here was to ascertain the consequences on τ_{fluo} . Lifetime analysis of L-PS serves as a way to probe the local microenvironment of photosensitive drugs in cell-like media. The companion work showed that HPPH was primarily localized in the liposome membrane,³² while Al-2 and Al-4 molecules reside predominantly at membrane interfaces and in the aqueous core, respectively. This microenvironment influences not only the PS physicochemical properties, such as aggregation, but should also affect the decay response. Here, we extended our studies of liposome-confined PS by probing the τ_{fluo} behavior associated with this localization. In measuring τ_{fluo} , one should be cautious about the absolute lifetime values and recognize that PS excitation itself may induce some photodynamic action that affects the local microenvironment (e.g., breaking of lipid membranes). However, upon comparison of the trends observed in liposomes, the tendencies were not toward free PS behavior and did not change over the measurement time. Thus, for the purpose of this study, we assumed such contributions were negligible. We examined the fluorescence decay of L-PS as a function of temperature and oxygen concentration and compared them to trends observed in free solution.

4.2 Effect of Confinement on Fluorescence Lifetime

Under ambient environmental conditions, both free Al-2 and Al-4 displayed longer τ_{fluo} values in comparison to the respective encapsulated L-PS solution [Figs. 2(a) and 2(b); Table 1]. Previous reports examining Al-2 fluorescence lifetimes in varying polarity solvents and in bacterial membranes show that longer lifetimes are typically observed in more polar environments.^{13,42} Furthermore, the lifetime of Al-2 in a confined liposome system can be reduced as much as 1 ns in L-Al-2 by reducing the phospholipid concentration in solution.¹³ Such chemical contributions can, for example, account for the longer lifetime observed here for free-solution Al-2 compared to L-Al-2—a case where the liposome concentration is low and where the local polarity is reduced upon integrating Al-2 in liposomes. However, for hydrophilic Al-4 the polarity of the microenvironment is not expected to significantly change upon incorporation into the aqueous core of the liposome. As previously established in the companion paper,³² the fluorescence of free-PS solutions at high concentrations can be significantly influenced by both chemical and optical phenomena (e.g., re-absorbed emission). At a high concentration of fluorescent Al-4 species, the companion work demonstrated a significant contribution from re-absorbed emission under minimally aggregated conditions.³²

It has been demonstrated that the phenomenon of re-absorption can result not only in significant redshifting of the emission,³² but re-emission can also lengthen the perceived τ_{fluo} .⁴³

A comparison of the goodness of fit of the lifetimes revealed interesting results arising from PS confinement. Comparing the fitted lifetime of solution-phase Al-2 versus L-Al-2 to a monoexponential model yielded a χ_R^2 value that increased by a factor of 2, suggesting that the fluorescence of L-Al-2 is more suitably described by a multiexponential decay model. The larger χ_R^2 result from monoexponential fitting of L-Al-2 may be related to the micro-heterogeneous distribution achieved upon associating with the liposome interface, as demonstrated in the companion work.³² A previous report demonstrated that the decay of Al-2 transforms from mono- to bi-exponential as phospholipid concentration is increased.¹³ This phenomenon is believed to be related to a change in how Al-2 interacts with its local environment as the medium transitions from a water to lipid phase. An increased contribution of biexponential behavior was also found when amphiphilic Al-2 was confined to bacterial membranes.¹³ These observations agree with the trend toward multiexponential behavior observed for Al-2 in this study when complexed to liposomes, a similar cell model. The presence of multiexponential dynamics can be rationalized further by considering the surface properties of the liposomal membrane, which facilitate interfacial interactions of amphiphilic Al-2 molecules at the bipolar surface.^{7,42} This interfacial arrangement can impart a highly dynamic and bipolar microenvironment associated with membrane motility and heterogeneity, subsequently leading to the multiexponential decay observed here for L-Al-2.

In the case of the more hydrophilic tetrasulfonated analog, Al-4, the favorable solubility of this compound in aqueous media imparts a lower degree of aggregation,⁴⁴ as demonstrated previously in the companion work.³² As such, good adherence to a monoexponential decay model was expected, even at high free-solution concentrations of $\sim 50 \mu\text{M}$.⁴² Our finding of a reduced χ_R^2 value by a factor of 5, in association with Al-4 encapsulation into the liposome core, suggests a more uniform and protected microenvironment was adopted upon encapsulation, and/or the PS concentration was reduced in L-Al-4. Both of these possibilities are consistent with the observed tendency toward monoexponential decay.¹³ Unlike amphiphilic Al-2, which exhibited reduced re-absorbed emission in the presence of nonfluorescent aggregates, the decay kinetics of solution-state Al-4 were more strongly governed by re-absorption, as shown in the companion work³² and by Pompa et al.⁴⁵ The greater influence of re-absorbed emission can account for the longer apparent lifetimes in solution Al-4. The re-absorbed emission contributed to the higher χ_R^2 results obtained in bulk compared to L-Al-4, since the re-emitted light was expected to result in a broader distribution of lifetimes.

The fluorescence decay of lipophilic HPPH had completely different dynamics from the amphiphilic or hydrophilic phthalocyanines examined. While membrane-bound L-HPPH is characterized by a nearly perfect monoexponential, τ_{fluo} of free-solution HPPH cannot be represented accurately by a single decay lifetime. This implies that incorporation into the bilayer membrane restricts L-HPPH to a homogenous

microenvironment. An eight-fold reduction in the χ_R^2 value upon fitting to a biexponential model suggests that solution-phase HPPH was represented better by two decay times from FD measurements at 661-nm excitation. In comparison, photon counting (at 400-nm excitation) was slightly more sensitive to FBS solvent autofluorescence in HPPH ($\leq 1\%$ of the signal), in part accounting for the multiexponential result observed in the TD. In the absence of autofluorescence, however, the two lifetimes of HPPH are distinguishably separated in time ($\tau_1 \sim 1 \text{ ns}$ and $\tau_2 \sim 5 \text{ ns}$) and likely arise from microenvironment heterogeneity and/or the presence of multiple molecular conformations, including aggregates. Given the high concentration of this hydrophobic species ($100 \mu\text{M}$), aggregates were prevalent in aqueous solution.³² Aggregates can produce microheterogeneity that contributes to the multiexponential behavior observed in free solution by both the TD and FD methods. Moreover, the significantly lower lifetimes observed in free-solution HPPH ($\tau_{\text{fluo}} \sim 5.6 \text{ ns}$, 1.1 ns) versus L-HPPH ($\tau_{\text{fluo}} \sim 8.3 \text{ ns}$) (Table 1) can be justified by the relatively high aggregate concentration of hydrophilic PS in aqueous media, since this can effectively quench the radiative decay. Significant reductions in τ_{fluo} due to aggregation are not uncommon, as supported by the previous observation of a 2-ns decrease in another photosensitizing porphyrin, mTHPC, from 7.5 ns (unaggregated state) to 5.5 ns (aggregated form).⁴⁶

4.3 Effect of Heating on Fluorescence Lifetime

Increasing the temperature of both free and liposome-confined PSs resulted in a decrease in the τ_{fluo} with the exception of hydrophobic HPPH in solution. As a physical effect, temperature elevation induces greater collisional relaxation of fluorescent molecules. However, one must also consider the chemical effects induced by heating. Specifically, heating increases the solubility constant (K_{sp}) for the PS molecules. As the solubility increases, the aggregated equilibrium is reduced, promoting kinetic “averaging” to a more uniform environment for the PS. This is evidenced by the reduction in χ_R^2 from monoexponential fitting, particularly for solution-phase Al-2 (previously shown to be highly aggregated at the experimental concentration).

In discussions relating heating effects to changes in τ_{fluo} properties, it is necessary to address the background effects that can obscure the data and lead to invalid conclusions. For example, heating can initiate liposome fusion to form larger vesicles. Changes in the background liposome scattering due to changes in liposome size must therefore be quantified. Analysis of the L-Blank “scattering lifetime” acquired from 30 to 78 °C showed an increase from 0.03 to 0.06 ns. The net change of 0.03 ns was on the order of the error and thus was considered negligible.

Heating of L-Al-2 yielded similar lifetime decreases to that observed in bulk-solution Al-2 up to 47 °C. Above this thermal breakpoint, we observed different decay responses to heat. Examination of the DSC scan of L-Blank [Fig. 2(c)] revealed a thermal phase transition of CHOL/DOPC vesicles occurring around 50 °C, near the breakpoint observed in τ_{fluo} in Fig. 2(a). (DSC is a common tool for examining phase transitions in materials.) Because the lifetime of L-Al-2 is dependant on its interfacial localization at the membrane sur-

face, the lifetime kinetics were correlated with the highly mobile nature of the bilayer. The presence of CHOL in the membrane further enhanced the dynamic nature of the bilayer.^{47,48} Thus, the fluorescence decay of purely membrane-bound L-AI-2 species should be influenced by the temperature-mediated membrane fluidity. Conversely, heating solution-phase AI-2 should predominantly affect aggregation and solubility. Since L-AI-2 is confined interfacially, we find that it shares both membrane-dependent lifetime kinetics as well as transitions related to solubility of aggregates in aqueous media up to the temperature marking the phase transition of the lipid.

For the most hydrophilic PS, both solution-phase AI-4 and L-AI-4 respond the same, as evidenced by the identical slopes in temperature curves of τ_{fluo} [Fig. 2(b)]. Thus, the encapsulation of AI-4 did not generate a different microenvironment that perturbed the temperature-dependent τ_{fluo} response. This result is in agreement with the localization studies of the companion work,³² which showed that the hydrophilic AI-4 preferentially partitioned to the aqueous core of liposomes. As such, AI-4 is expected to retain similar fluorescence decay dynamics once sequestered into similar aqueous media comprising the liposome core.

The temperature response of τ_{fluo} for lipophilic HPPH in solution has different characteristics than for hydrophilic AI-4 and amphiphilic AI-2. Specifically, the measured lifetime increases with increasing temperature, as indicated by the left shift of the phase curves. Heating HPPH does not appear to promote quenching as observed in AI-4 and AI-2. Therefore, the τ_{fluo} temperature curve produced by HPPH is not described simply by heat-induced collisional relaxation processes. Since the phase shifts in HPPH are not superimposable, the same exponential model cannot accurately represent the decay behavior over the temperature range examined. This can be interpreted as changes to the molecule (e.g., its conformation or aggregation) and/or its local environment imposed by temperature elevation. In a highly aggregating aqueous medium, heating can have a greater effect on the solubility of hydrophobic HPPH, thus reducing aggregation and increasing the lifetime. When confined to liposomes, L-HPPH is sequestered to a thermodynamically favorable bilayer phase. Here, aggregation was significantly reduced, and the expected temperature trend attributed to heat-induced quenching was recovered.

The vastly different lifetime behavior resulting from preferential localization of HPPH to the liposome bilayer [Figs. 2(c) and 2(d); Table 1] provokes questions regarding the consequences of the interaction between HPPH and unsaturated DOPC, which can be addressed with DSC. Membranes comprised of DOPC, and particularly those incorporating CHOL, are relatively disordered and have intrinsic mobility in the bilayer.^{47,48} DSC analysis showed that the phase transition temperature increases from 50 to 68 °C due to membrane inclusion of HPPH. This suggests that the incorporation of HPPH in the bilayer enhances the order and stability of the membrane. Consequently, the onset of thermal transition is at a temperature 18 °C higher than the blank liposome. Whether the application of liposomes is drug delivery or as cell phantoms to model photodynamic responses, these results imply that controlled vesicle properties are not only retained but

stabilized over high temperatures due to membrane incorporation of a hydrophobic PS.

4.4 Effect of Deoxygenation on Fluorescence Lifetime

Oxygen molecules are small, nonpolar quenchers that diffuse rapidly in most solvents, including water. The reduction in the measured dissolved oxygen concentration from 190 to 0.19 μM indicated that effective deoxygenation of the PS and L-PS solutions was achieved, irrespective of the medium viscosity. The measured τ_{autofluo} from L-Blank (inset Fig. 4) showed no dependence on oxygen concentration. This result suggests two things: (1) liposome scattering and autofluorescence lifetime were not affected by the deoxygenation process (i.e., the physical effects of photon migration remain the same), and (2) while oxygen may be a small, freely diffusing quencher in solution, the purging process (which effectively removes oxygen from the bulk aqueous solution) did not significantly alter the optically detected properties of the blank liposome membrane. Therefore, observed changes in fluorescent lifetime due to deoxygenation must arise from the PS in its specific environment.

The membrane-embedded-PS, L-HPPH, exhibited little sensitivity in fluorescence to a reduction in the aqueous oxygen concentration, as indicated by the small change in lifetime from 7.67 ns to 7.62 ns upon deoxygenation (Table 1). The concentration of oxygen within fluid phosphatidylcholine membranes, similar to DOPC, was a diffusion-solubility product.⁴⁹ The solubility of oxygen in membranes is four-fold higher than in water, favoring concentration in hydrophobic media. The diffusion coefficient of oxygen is 20% of that in water, while the lipid-water partition coefficient is approximately 5.³⁹ Therefore, in traversing the thin membrane (~ 4 nm) of the liposomes,⁵⁰ the membrane permeability (defined as the product of the quenching constant times the oxygen diffusion coefficient, over the thickness) suggests that the liposome bilayer is not a diffusion barrier to oxygen.³⁹ Considering oxygen solely as a collisional quencher, the small change in τ_{fluo} due to deoxygenating L-HPPH was unexpected. In fact, the L-PS systems that showed the largest lifetime changes in response to oxygen concentration were L-AI-2 and L-AI-4 (Table 1), i.e., the PSs that are in part or predominantly confined to the aqueous phase of the liposome. Interfacial L-AI-2 was most sensitive, with a pronounced difference in the measured lifetime of 0.53 ns associated with deoxygenation. The differences in the magnitude of the lifetime shift in response to oxygen depletion in L-PS are PS-dependent and do not correlate to the trends observed in the corresponding bulk solutions. Thus, oxygen is not simply involved in quenching, but in fact modifies the PS environment to a degree that depends on the PS localization.

The unexpected decrease in τ_{fluo} exhibited by the liposomal-phthalocyanines (L-AI-2, L-AI-4) after Ar deoxygenation is curious and merits further discussion. This reduction in lifetime was not seen in the free-solution analogs, indicating that Ar purging had very different effects on L-PS and bulk-PS solutions. Experimentally, the Ar pressure was kept very low during purge, and the τ_{fluo} shifts observed in deoxygenated L-PS solutions were not in the direction of bulk-solution PS. Therefore, this effect cannot be rationalized by liposome rupture due to inadvertent lipid peroxidation,

photo-initiated by lifetime measurements. However, inspection of the DC magnitude (FD measurements) and the photon counts (TD experiments), revealed that Ar purging resulted in a significant and reproducible decrease in fluorescence intensity for both L-AI-2 and L-AI-4 solutions (Table 1). These photophysical changes suggest a photochemical side-reaction or change in the molecular structure caused by deoxygenation in liposomes L-AI-2 and L-AI-4. For example, a possible byproduct of deoxygenation may be a change in the dimeric complex known as the μ -oxo aggregate. Such “contact dimers” have been reported for aluminum and zinc phthalocyanine sulfonates in which the phthalocyanine molecules were linked chemically via the oxygen atom and known to depend on the solvent environment.^{14,51,52} Previous studies of the PS mTHPC confined in intracellular environments showed that oxygen concentration had a complex effect on PS photochemistry and photobleaching properties.⁵³ Hence, simple quenching processes cannot adequately describe the oxygen-dependent τ_{fluo} response observed here with L-AI-2 and L-AI-4. We are currently investigating the complex role of oxygen on L-PS photochemical properties using spectroscopic methods over a broad range of oxygen concentrations.

Unlike the confined PS analogs, the lifetimes of free-solution PSs did not decrease with Ar deoxygenation. Instead, a small but expected increase in fluorescent lifetime was associated with the removal of oxygen, indicative of quencher depletion. The small magnitude of this change in deoxygenating bulk PS is not surprising given that the bulk solutions are significantly higher in concentration. The spectroscopic study of the companion work showed that the fluorescence of bulk solutions at high PS concentrations was dominated by either aggregation and/or re-absorption of emission effects.³² Thus, at high concentrations, quantifying oxygen-related quenching contributions to τ_{fluo} shifts in PS solution is not trivial. Despite this, the critical result remains that the τ_{fluo} response to oxygen depletion in highly concentrated PS solutions appears independent of the PS type, unlike the result in the encapsulated scheme. The implication is that oxygen concentration has very different photophysical consequences for free PS compared to PS confined in intracellular environments.

5 Conclusions

We have studied the photophysical consequences of confining three PSs of varying hydrophobicity, AI-2, AI-4, and HPPH, in cell-like liposome constructs. As measured through τ_{fluo} , the selective molecular affinity of a PS to either the core, interface, or membrane constituents of liposomes sequestered some PSs to different microenvironments. This chemically driven confinement produced significantly different photophysical properties compared to PSs in free aqueous solution. The impact of localization on the fluorescence decay was examined as a function of heat or oxygen concentration. The photothermal response of hydrophilic and amphiphilic PSs confined in liposomes, such as AI-4 and AI-2, in part mimicked the lifetime kinetics observed in free solution. This was due to preferential PS-liposome interactions that facilitated complete or interfacial exposure to aqueous media. Conversely, the outcome of integrating highly lipophilic molecules in liposomes (i.e., HPPH) was a reduction in the local

heterogeneity due to molecular localization in the vesicle bilayer. In such a case, the photothermal fluorescence decay kinetics were significantly different than in bulk solution. This is because heating had different consequences for PS versus L-PS due to the relative contribution of solubility and collisional quenching effects. Lastly, photo-oximetric measurements of τ_{fluo} , performed as a function of the solvent oxygen concentration, revealed that oxygen depletion in free-PS solution effectively increased the lifetimes for all PSs due to the absence of oxygen quenchers. Conversely, oxygen depletion in L-PS solutions lengthened the τ_{fluo} to an extent that was dependent on the nature of the PS confinement and could not be explained by quenching arguments. Monitoring of the photo-thermal and -oximetric fluorescence decay properties of PSs in simplified cell models, like liposomes, facilitates the understanding of photophysical responses produced by sensitizers in different cellular microenvironments. This information is valuable for the molecular design of more effectively targeted PDT drugs.

Acknowledgments

This work was financially supported in part by Canadian Institutes of Health Research (CIHR) and CIHR (IG) RMS-79069. We are grateful to Dr. Barbara Henderson and the Photodynamic Therapy Center of Roswell Park Cancer Institute for providing HPPH. We thank Prof. Adi Eisenberg, Prof. Carl Bartels, and Dr. Anja Kroeger of McGill University Chemistry for assistance with DLS.

References

1. L. I. Grossweiner, “Photodynamic therapy: science and technology,” Chapter 10 in *The Science of Phototherapy: An Introduction*, L. R. Jones, J. B. Grossweiner, and B. H. G. Rogers, Eds., pp. 243–275, Springer, Norwell, MA (2005).
2. T. J. Dougherty, C. J. Gomer, B. W. Henderson, G. Jori, D. Kessel, M. Koberlik, J. Moan, and Q. Peng, “Photodynamic therapy,” *J. Natl. Cancer Inst.* **90**(12), 889–905 (1998).
3. E. Reddi and G. Jori, “Steady-state and time-resolved spectroscopic studies of photodynamic sensitizers: porphyrins and phthalocyanines,” *Rev. Chem. Intermed.* **10**(3), 241–268 (1988).
4. I. J. MacDonald, J. Morgan, D. A. Bellnier, G. M. Paszkiewicz, J. E. Whitaker, D. J. Litchfield, and T. J. Dougherty, “Subcellular localization patterns and their relationship to photodynamic activity of pyropheophorbide-*a* derivatives,” *Photochem. Photobiol.* **70**(5), 789–797 (1999).
5. G. Kramer-Marek, C. Serpa, A. Szurko, M. Widel, A. Sochanik, M. Sniatura, P. Kus, R. M. D. Nunes, L. G. Arnaut, and A. Ratuszna, “Spectroscopic properties and photodynamic effects of new lipophilic porphyrin derivatives: efficacy, localization and cell death pathways,” *J. Photochem. Photobiol., B* **84**(1), 1–14 (2006).
6. A. A. Rosenkranz, D. A. Jans, and A. S. Sobolev, “Targeted intracellular delivery of photosensitizer to enhance photodynamic efficiency,” *Immunol. Cell Biol.* **78**(4), 452–464 (2000).
7. I. J. MacDonald and T. J. Dougherty, “Basic principles of photodynamic therapy,” *J. Porphy. Phthalocyanines* **5**(2), 105–129 (2001).
8. D. Kessel and Y. Luo, “Intracellular sites of photodamage as a factor in apoptotic cell death,” *Photochem. Photobiol.* **5**(2), 181–184 (2001).
9. Y. You, S. L. Gibson, R. Hilf, S. R. Davies, A. R. Oseroff, I. Roy, T. Y. Ohulchansky, E. J. Bergey, and M. R. Detty, “Water soluble, core-modified porphyrins. 3. Synthesis, photophysical properties, and *in vitro* studies of photosensitization, uptake, and localization with carboxylic acid-substituted derivatives,” *J. Med. Chem.* **46**(17), 3734–3747 (2003).
10. K. Lang, J. Mosinger, and D. M. Wagnerová, “Photophysical properties of porphyrinoid sensitizers non-covalently bound to host molecules; models for photodynamic therapy,” *Coord. Chem. Rev.* **248**(3–4), 321–350 (2004).

11. C. M. Allen, R. Langlois, W. M. Sharman, C. La Madeleine, and J. E. Van Lier, "Photodynamic properties of amphiphilic derivatives of aluminum tetrasulfophthalocyanine," *Photochem. Photobiol.* **76**(2), 208–216 (2002).
12. A. Rosenfeld, J. Morgan, L. N. Goswami, T. Ohulchanskyy, X. Zheng, P. N. Prasad, A. Oseroff, and R. K. Pandey, "Photosensitizers derived from 13²-oxo-methyl pyropheophorbide-a: enhanced effect of indium(III) as a central metal in *in vitro* and *in vivo* photosensitizing efficacy," *Photochem. Photobiol.* **82**(3), 626–634 (2006).
13. J. A. Lacey and D. Phillips, "Fluorescence lifetime measurements of disulfonated aluminum phthalocyanine in the presence of microbial cells," *Photochem. Photobiol. Sci.* **1**(6), 378–383 (2002).
14. N. A. Kuznetsova, N. S. Gretsova, V. M. Derkacheva, S. A. Mikhalenko, L. I. Solov'eva, O. A. Yuzhakova, O. L. Kaliya, and E. A. Luk'yanets, "Generation of singlet oxygen with anionic aluminum phthalocyanines in water," *Russ. J. Gen. Chem.* **72**(2), 300–306 (2002).
15. S. Fitzgerald, C. Farren, C. F. Stanley, A. Beeby, and M. R. Bryce, "Fluorescent phthalocyanine dimers—a steady state and flash photolysis study," *Photochem. Photobiol. Sci.* **1**(8), 581–587 (2002).
16. R. Roy, A. Godavarty, and E. M. Sevick-Muraca, "Fluorescence-enhanced three-dimensional lifetime imaging: a phantom study," *Phys. Med. Biol.* **52**(14), 4155–4170 (2007).
17. R. Richards-Kortum and E. M. Sevick-Muraca, "Quantitative optical spectroscopy for tissue diagnosis," *Annu. Rev. Phys. Chem.* **47**(1), 555–606 (1996).
18. B. W. Henderson and S. O. Gollnick, "Mechanistic principles of photodynamic therapy," Chapter 36 in *Biomedical Photonics Handbook*, T. Vo-Dinh, Ed., pp. 36-1–36-14, CRC Press, Oak Ridge, TN (2003).
19. J. Lasch, V. Weissig, and M. Brandl, "General methods: preparation of liposomes," Chapter 1 in *Liposomes: A Practical Approach*, V. Torchilin and V. Weissig, Eds., pp. 3–27, Oxford University Press, New York (2003).
20. B. Chen, B. W. Pogue, and T. Hasan, "Liposomal delivery of photosensitizing agents," *Expert Opinion* **2**(3), 477–487 (2005).
21. F. Riechelli, S. Gobbo, G. Moreno, C. Salet, L. Brancalione, and A. Mazzini, "Photophysical properties of porphyrin planar aggregates in liposomes," *Eur. J. Biochem.* **253**(3), 760–765 (1998).
22. M. Hoebeke and X. Damoiseau, "Determination of the singlet oxygen quantum yield of bacteriochlorin: a comparative study in phosphate buffer and aqueous dispersion of dimristoyl-L-phosphatidylcholine liposomes," *Photochem. Photobiol. Sci.* **1**(4), 283–287 (2002).
23. Ž. Lukšienė, "Photodynamic therapy: mechanism of action and ways to improve the efficiency of treatment," *Medicina* **39**(12), 1137–1150 (2003).
24. M. R. Horsman, "Tissue physiology and the response to heat," *Int. J. Hyperthermia* **22**(3), 197–203 (2006).
25. E. Glassberg, L. Lewandowski, C. Halcin, G. Lask, and J. Uitto, "Hyperthermia potentiates the effects of aluminum phthalocyanine tetrasulfonate-mediated photodynamic toxicity in human malignant and normal cell lines," *Lasers Surg. Med.* **11**(5), 432–439 (1991).
26. D. L. Liu, S. Andersson-Engels, C. Sturesson, K. Svanberg, C. H. Håkansson, and S. Svanberg, "Tumour vessel damage resulting from laser-induced hyperthermia alone and in combination with photodynamic therapy," *Cancer Lett.* **111**(1–2), 157–165 (1997).
27. H. K. Biesalski and J. Frank, "Combination of PDT and HT increases free radical induced tumor cell death *in vivo*," *FASEB J.* **20**, A149–A150 (2006).
28. A. M. Ponce, Z. Vujaskovic, F. Yuan, D. Needham, and M. W. Dewhirst, "Hyperthermia mediated liposomal drug delivery," *Int. J. Hyperthermia* **22**(3), 205–213 (2006).
29. B. W. Henderson and V. H. Fingar, "Oxygen limitation of direct tumor cell kill during photodynamic treatment of a murine tumor model," *Photochem. Photobiol.* **49**(3), 299–304 (1989).
30. V. H. Fingar, "Vascular effects of photodynamic therapy," *J. Clin. Laser Med. Surg.* **14**(5), 323–328 (1996).
31. A. Lavi, H. Weitman, R. T. Holmes, K. M. Smith, and B. Ehrenberg, "The depth of porphyrin in a membrane and the membrane's physical properties affect the photosensitizing efficiency," *Biophys. J.* **82**(4), 2101–2110 (2002).
32. I. Noiseux, O. Mermut, J. P. Bouchard, J. F. Cormier, P. Desroches, M. Fortin, P. Gallant, S. Leclair, M. L. Vernon, K. R. Diamond, and M. S. Patterson, "Effect of liposomal confinement on photochemical properties of photosensitizers with varying hydrophilicity," *J. Biomed. Opt.* **13**, 0413xx (2008).
33. A. J. Jin, D. Huster, K. Gawrisch, and R. Nossal, "Light scattering characterization of extruded lipid vesicles," *Eur. Biophys. J.* **28**(3), 187–199 (1999).
34. D. G. Hunter and B. J. Frisken, "Effect of extrusion pressure and lipid properties on the size and polydispersity of lipid vesicles," *Biophys. J.* **74**(6), 2996–3002 (1998).
35. R. L. Biltonen and D. Lichtenberg, "The use of differential scanning calorimetry as a tool to characterize liposome preparations," *Chem. Phys. Lipids* **64**(1–3), 129–142 (1993).
36. R. H. Mayer, J. S. Reynolds, and E. M. Sevick-Muraca, "Measurement of the fluorescence lifetime in scattering media by frequency-domain photon migration," *Appl. Opt.* **38**(22), 4930–4938 (1999).
37. J. R. Lackowitz, "Time-domain lifetime measurements, frequency-domain lifetime measurements, and advanced topics in fluorescence quenching," Chapters 4, 5, and 9 in *Principles of Fluorescence Spectroscopy*, pp. 95–162, 267–278, Kluwer Academic/Plenum, New York (1999).
38. D. A. Turtton, G. D. Reid, and G. S. Beddard, "Accurate analysis of fluorescence decays from single molecules in photon counting experiments," *Anal. Chem.* **75**(16), 4182–4187 (2003).
39. S. Kölchens, V. Ramaswami, J. Birgenheier, L. Nett, and D. F. O'Brien, "Quasi-elastic light scattering determination of the size distribution of extruded vesicles," *Chem. Phys. Lipids* **65**(1), 1–10 (1993).
40. W. H. Press, B. P. Flannery, S. A. Teukolsky, and W. T. Vetterling, "Modeling of data," Chapter 14 in *Numerical Recipes: The Art of Scientific Computing*, pp. 498–539, Cambridge University Press, Cambridge, NY (1986).
41. I. Bronshtein, M. Afri, H. Weitman, A. A. Frimer, K. M. Smith, and B. Ehrenberg, "Porphyrin depth in lipid bilayers as determined by iodide and parallax fluorescence quenching methods and its effect on photosensitizing efficiency," *Biophys. J.* **87**(2), 1155–1164 (2004).
42. S. Dhami, J. J. Cosa, S. M. Bishop, and D. Phillips, "Photophysical characterization of sulfonated aluminum phthalocyanines in a cationic reversed micellar system," *Langmuir* **12**(2), 293–300 (1996).
43. J.-F. Cormier, M. Fortin, J. Fréchette, I. Noiseux, M. L. Vernon, and W. Long, "The effects of self-absorption and detection geometry on fluorescence intensity and decay lifetime," *Proc. SPIE* **5702**, 123–134 (2005).
44. P. Juzenas, A. Juzeniene, R. Rotomskis, and J. Moan, "Spectroscopic evidence of monomeric aluminium phthalocyanine tetrasulfonate in aqueous solutions," *J. Photochem. Photobiol., B* **75**(1–2), 107–110 (2004).
45. P. P. Pompa, G. Ciccarella, J. Spadavecchia, R. Cingolani, G. Vasapollo, and R. Rinaldi, "Spectroscopic investigation of inner filter effects by phthalocyanine solutions," *J. Photochem. Photobiol., A* **163**(1–2), 113–120 (2004).
46. M. Kress, T. Meier, R. Steiner, F. Dolp, R. Erdmann, U. Ortmann, and A. Rück, "Time-resolved microspectrofluorometry and pulsed diode lasers in laser scanning microscopes," *J. Biomed. Opt.* **8**(1), 26–32 (2003).
47. P. L. Yeagle, "Cholesterol and the cell membrane," *Biochim. Biophys. Acta* **822**(3–4), 267–287 (1985).
48. A. Filippov, G. Orädd, and G. Lindblom, "The effect of cholesterol on the lateral diffusion of phospholipids in oriented bilayers," *Biophys. J.* **84**(5), 3079–3086 (2003).
49. W. K. Subczynski, J. S. Hyde, and A. Kusumi, "Oxygen permeability of phosphatidylcholine-cholesterol membranes," *Proc. Natl. Acad. Sci. U.S.A.* **86**(12), 4474–4478 (1989).
50. J. Gallová, D. Uhríková, A. Islamov, A. Kuklin, and P. Balgavý, "Effect of cholesterol on the bilayer thickness in unilamellar extruded DLPC and DOPC liposomes: SANS contrast variation study," *Gen. Physiol. Biophys.* **23**(1), 113–128 (2004).
51. P. C. Martin, M. Gouterman, B. V. Pepich, G. E. Renzoni, and D. C. Schindele, "Effect of ligands, solvent, and variable sulfonation on dimer formation of aluminum and zinc phthalocyaninesulfonates," *Inorg. Chem.* **30**(17), 3305–3309 (1991).
52. M. J. Stillman and T. Nyokong, "Absorption and magnetic circular dichroism spectral properties of phthalocyanines," Chapter 3 in *Phthalocyanines: Properties and Applications*, C. C. Leznoff and A. B. P. Lever, Eds., Vol. 1, pp. 202–207, VCH, New York (1989).
53. L. Kunz, J. Alexander, and J. MacRobert, "Intracellular photobleaching of Foscan exhibits a complex dependence on oxygen level and fluence rate," *Photochem. Photobiol.* **75**(1), 28–35 (2002).